International Journal of Biological Macromolecules 258 (2024) 128793

Contents lists available at ScienceDirect

International Journal of Biological Macromolecules

journal homepage: www.elsevier.com/locate/ijbiomac

Electrospun *Tamarindus indica*-loaded antimicrobial PMMA/cellulose acetate/PEO nanofibrous scaffolds for accelerated wound healing: *In-vitro* and *in-vivo* assessments

Shaimaa S. Goher [a], Shaza H. Aly [b], Marwa M. Abu-Serie [c], Shahira H. EL-Moslamy [d], Ayat A. Allam [e,f], Nadeen H. Diab [g], Khaled M.A. Hassanein [h], Rana A. Eissa [i], Noura G. Eissa [i,j], Mahmoud Elsabahy [i,k,*], Elbadawy A. Kamoun [l,m,*]

[a] *Nanotechnology Research Centre (NTRC), The British University in Egypt (BUE), Suez Desert Road, El Sherouk City, Cairo 1183, Egypt*
[b] *Department of Pharmacognosy, School of Pharmacy, Badr University in Cairo, Badr City, Cairo 11829, Egypt*
[c] *Medical Biotechnology Department, Genetic Engineering and Biotechnology Research Institute (GEBRI), City of Scientific Research and Technological Applications (SRTA-City), New Borg Al-Arab, Alexandria 21934, Egypt*
[d] *Bioprocess Development Department (BID), Genetic Engineering and Biotechnology Research Institute (GEBRI), City of Scientific Research and Technological Applications (SRTA-City), New Borg El-Arab City, Alexandria 21934, Egypt*
[e] *Department of Pharmaceutics, Faculty of Pharmacy, Assiut University, Assiut 71526, Egypt*
[f] *Department of Pharmaceutics, Faculty of Pharmacy, Sphinx University, Assiut 71515, Egypt*
[g] *Department of Pharmacognosy, Faculty of Pharmacy, Assiut university, Assiut 71526, Egypt*
[h] *Pathology and Clinical Pathology Department, Faculty of Veterinary Medicine, Assiut University, Assiut 71526, Egypt*
[i] *Badr University in Cairo Research Center, Badr University in Cairo, Badr City, Cairo 11829, Egypt*
[j] *Department of Pharmaceutics, Faculty of Pharmacy, Zagazig University, Zagazig 44519, Egypt*
[k] *Department of Chemistry, Texas A&M University, College Station, TX 77842, USA*
[l] *Polymeric Materials Research Dep., Advanced Technology and New Materials Research Institute (ATNMRI), City of Scientific Research and Technological Applications (SRTA-City), Alexandria 21934, Egypt*
[m] *Biomaterials for Medical and Pharmaceutical Applications Research Group, Nanotechnology Research Center (NTRC), The British University in Egypt (BUE), Cairo 11837, Egypt*

ARTICLE INFO

Keywords:
Nanofibers
Electrospinning
Wound healing
Wound dressing
Tamarindus indica
PMMA
PEO
Cellulose acetate
Antimicrobial
In vitro
In vivo

ABSTRACT

In this work, *Tamarindus indica* (*T. indica*)-loaded crosslinked poly(methyl methacrylate) (PMMA)/cellulose acetate (CA)/poly(ethylene oxide) (PEO) electrospun nanofibers were designed and fabricated for wound healing applications. *T. indica* is a plant extract that possesses antidiabetic, antimicrobial, antioxidant, antimalarial and wound healing properties. *T. indica* leaves extract of different concentrations were blended with a tuned composition of a matrix comprised of PMMA (10 %), CA (2 %) and PEO (1.5 %), and were electrospun to form smooth, dense and continuous nanofibers as illustrated by SEM investigation. *In vitro* evaluation of *T. indica*-loaded nanofibers on normal human skin fibroblasts (HBF4) revealed a high compatibility and low cytotoxicity. *T. indica*-loaded nanofibers significantly increased the healing activity of scratched HBF4 cells, as compared to the free plant extract, and the healing activity was significantly enhanced upon increasing the plant extract concentration. Moreover, *T. indica*-loaded nanofibers demonstrated significant antimicrobial activity *in vitro* against the tested microbes. *In vivo*, nanofibers resulted in a superior wound healing efficiency compared to the control untreated animals. Hence, engineered nanofibers loaded with potent phytochemicals could be exploited as an effective biocompatible and eco-friendly antimicrobial biomaterials and wound healing composites.

1. Introduction

Various degrees of skin damage could occur due to surgical operations, burns, chemical injuries, ulcer, *etc.* Acute wounds (*e.g.*, surgical, and traumatic wounds, abrasions, and burns) and chronic wounds (*e.g.*, diabetic foot ulcers and pressure ulcers) are the main two

* Corresponding authors.
E-mail addresses: mahmoud.elsabahy@buc.edu.eg (M. Elsabahy), elbadawy.kamoun@bue.edu.eg (E.A. Kamoun).

https://doi.org/10.1016/j.ijbiomac.2023.128793
Received 3 August 2023; Received in revised form 10 December 2023; Accepted 12 December 2023
Available online 20 December 2023

categories of skin wounds, where treatment depends on the depth, size and extent of the wound [1]. Wound healing is a dynamic complicated process of tissue regeneration, which occur over four stages: hemostasis, inflammation, proliferation and remodeling [2]. Despite the spontaneous skin repair mechanism, bacterial infections are always among the main reasons for wound healing delaying [2]. Wound dressings were developed as an efficient tool of managing the wound healing process [3]. Currently, efforts in developing skin tissue engineered materials are directed towards the fabrication of 3D micro- and nano-fibrous materials that mimic the extracellular matrix of natural skin.

Various techniques and methods were developed to fabricate nanofibers using both electrospinning and non-electrospinning techniques [4]. Electrospinning techniques are commonly used owing to their effectiveness in the production of nanoscale fibers with larger surface area, enhanced interconnectivity and structural stability [4–7]. Characteristics of the collected fiber mainly depends on the electrospinning environment, parameters, and the blend solution characteristics [8–11]. Development of nanofiber dressings involve various natural (*e.g.*, hyaluronic acid, cellulose, gelatin, collagen, *etc.*) and/or synthetic polymers (*e.g.,* poly(lactic acid), poly(lactic-*co*-glycolic acid), poly(ε-caprolactone) [10–13].

Poly(methyl methacrylate) (PMMA) is a transparent glassy thermoplastic amorphous hydrophobic polymer that exhibits biocompatibility and decent processing conditions. However, biomedical applications of PMMA are restricted by its low mechanical strength and brittleness [14]. On contrary, poly(ethylene oxide) (PEO) is a hydrophilic crystalline thermoplastic polymer that is available in various molecular weights. Cellulose acetate (CA) is a natural inexpensive cellulose derivative that is widely available and exists in the cell wall of green plants. CA nanofibers are biodegradable and biocompatible with high porosity, good air permeability and stable chemical properties. Hence, it is being used in several biomedical applications [15–17].

Tamarindus indica (Tamarind) possesses antidiabetic, antimicrobial, antioxidant, antimalarial, and other therapeutic effects, and it has been widely utilized in traditional medicine for management of wounds to promote healing and mitigate inflammation [18]. *Tamarindus indica* trees belong to a globally distributed family known as *Fabaceae* (bean family), originally located in Africa [19]. Tamarind is a reservoir for many phototherapeutics such as phenolic compounds like procyanidin B2, catenin, tartaric acid, pectin, mucilage, carbohydrates, *etc.* [19]. Leaves are more abundant than other plant parts and have higher phenolic content than other parts [20].

Nanomaterials of various compositions have been exploited for topical antimicrobial, hemostatic and wound healing applications, due to their ability to provide an enhanced surface area and stability for their loaded cargoes [21–24]. For instance, nanofibers could provide significant ability to expedite the healing process *in vivo* and antibacterial dressings in several wound healing applications [21,25–27]. Among the multiple synthetic and natural therapeutics that were included in the composition of nanofibers, plant extract of *T. indica* has not been tested yet.

In the present study, newly designed electrospun PMMA/CA/PEO nanofibrous scaffolds mats were loaded with different concentrations of *T. indica* plant extract. Separation, characterizations, and structure elucidation of *T. indica* plant extract, and the fabrication process of the therapeutic electrospun nanofibers were assessed in detail. Additionally, the free and nanofiber-loaded plant extract were assessed for their antimicrobial and wound healing activities, both *in vitro, and in vivo.*

2. Materials and methods

2.1. Materials

Poly(methyl methacrylate) (PMMA, M_w ~ 550 kDa) and poly (ethylene oxide) (PEO, M_n ~ 30,000) were purchased from Merck (Darmstadt, Germany). Cellulose Acetate (CA, M_n ~ 30,000) was purchased from Alpha Chemika (Mumbai, India), *N,N*-dimethylformamide (DMF, > 99 %) was obtained from Fisher Chemicals (Hampton, NH). All reagents were used as received without further purification. *Tamarindus indica* (Fabaceae) leaves were collected from the Zoo Botanical Garden (Giza, Egypt), in October 2021. The leaves were kindly identified and authenticated by the agricultural engineer Terase Labib, consultant of Plant Taxonomy at the Ministry of Agriculture and El-Orman Botanical Garden. Voucher specimens were deposited under code BUC-PHG-TIL-6 in the Department of Pharmacognosy, Faculty of Pharmacy, Badr University in Cairo (Cairo, Egypt).

2.2. Preparation of T. indica plant extract

Air-dried leaves of *T. indica* (200 g) were powdered and defatted with *n*-hexane (1 L × 3) followed by filtration to yield 1.20 g of *n*-hexane fraction, followed by maceration in aqueous methanol (80 %) and the process was repeated 3 × till exhaustion. The combined filtered extracts were concentrated and dried under reduced pressure (45 °C) using a Rotavap (Buchi Rotavapor R-114 coupled with Buchi Vac. V-500 pump, Switzerland). After complete drying and lyophilization, the extraction yield from *T. indica* leaves was about 14.07 g (7.035 *w/w* %). The dried extract was kept at −20 °C until further analysis. The instrumental characterization of the plant extract (*i.e.*, UPLC-ESI-MS/MS, ^{1}H NMR and FTIR analyses) are discussed in detail in the Supplementary Materials (*Section S1*).

2.3. Electrospinning solutions preparation

2.3.1. PMMA/CA nanofiber optimization

PMMA solution (10 % *w/v*) and CA solution (2 and 5 % *w/v*) were prepared by dissolving in DMF, and solutions were kept under stirring overnight at 500 rpm at room temperature. Polymer blend solution (PMMA/CA) was prepared by mixing PMMA and CA at volume ratios of 90:10, 80:20 and 60:40 (*v/v*) and allowed to stir at room temperature for 2 h at 500 rpm to obtain a homogenous solution. The homogenous PMMA/CA solutions were fabricated into nanofibers using Electrospinner (MECC, NANON-01A, MECC, Japan) to select the optimal combination and spinning conditions. The homogeneous mixtures were placed into a 5 mL syringe (equipped with a 22G needle). Electrospinning parameters were varied where the feeding rate ranged from 0.5 to 1.2 mL/h, the applied voltage of 16–20 kV, and the tip to collector distance was 12 cm, while all electrospinning experiments were performed at ambient conditions with humidity of ~55 % (Table S1, Supplementary Materials). Moreover, Drum collector and a stationary rectangular metal collector (15–20 cm) covered by a piece of aluminum foil were used for the nanofiber deposition. Produced nanofibers were thermally treated at 80 °C for 12 h. The most uniform, reproducible, and bead-free nanofibers were obtained at a feed rate of 1 mL/h and applied voltage of 20 kV. Therefore, these parameters were kept constant for the studied polymer solutions.

2.3.2. Fabrication of PMMA/CA/PEO and T. indica loaded-PMMA/CA/PEO nanofibers

PEO was added to the optimized PMMA/CA polymer solution (60,40) at various concentrations (0.5, 1, 1.5, 2 and 3 % *w/v*). After addition, the mixture was allowed to stir for additional 2 h at room temperature at 500 rpm till the formation of a homogenous PMMA/CA/PEO blend solution. The blend mixture was electrospun at the previously established parameters (applied voltage 20 kV, feed rate 1 mL/h, drum speed 600–800 rpm, spinneret speed 100, spinneret width 15 mm at a distance of 12 cm).

PMMA/CA/PEO/*T. indica* nanofibers were fabricated by dissolving the plant extract *T. indica* at different concentrations (0.01, 0.015 and 0.02 %, *w/v*) in PEO (1.5 %, *w/v*)/PMMA/CA (60,40) before electrospinning at room temperature, using the aforementioned electrospinning parameters.

Table 1
Control untreated animals, and animals treated with plain nanofibers and nanofibers loaded with increasing concentrations of the plant extract.

Group	Plant extract (mg)	PEO (% *w/v*)	PMMA:CA (*v/v*)
Control	–	–	–
Group I	–	1.5	60:40
Group II	100	1.5	60:40
Group III	150	1.5	60:40
Group IV	200	1.5	60:40

2.4. Characterizations of plant extract and nanofibers

The instrumental characterizations of plant extract and nanofiber were discussed in detail in the Supplementary Materials (*Sections S1 and S2*).

2.5. In vitro bio-evaluations

The antimicrobial assays (broth dilution, biofilm inhibition and time-kill kinetics) and *in vitro* cell culture assays (cytotoxicity and scratch wound healing*)* were performed, and methodology is discussed in detail in the Supplementary Materials (Sections S3 and S4).

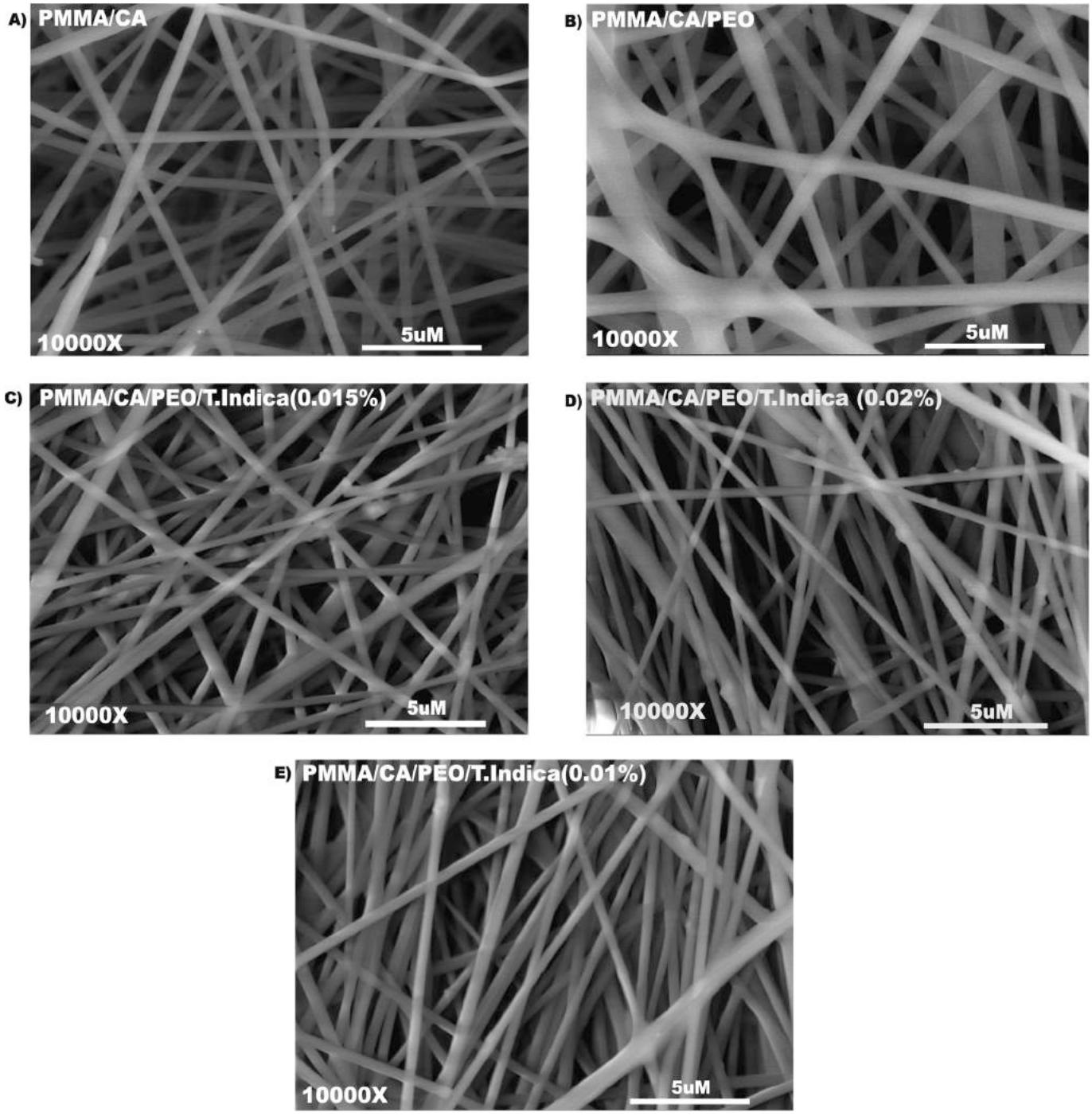

Fig. 1. SEM photographs of electrospun nanofibers of (A) PMMA/CA, PMMA/CA/PEO (B), *T. indica*-loaded PMMA/CA/PEO at various concentrations (0.01, 0.015, and 0.02 %) (C, D and E), respectively.

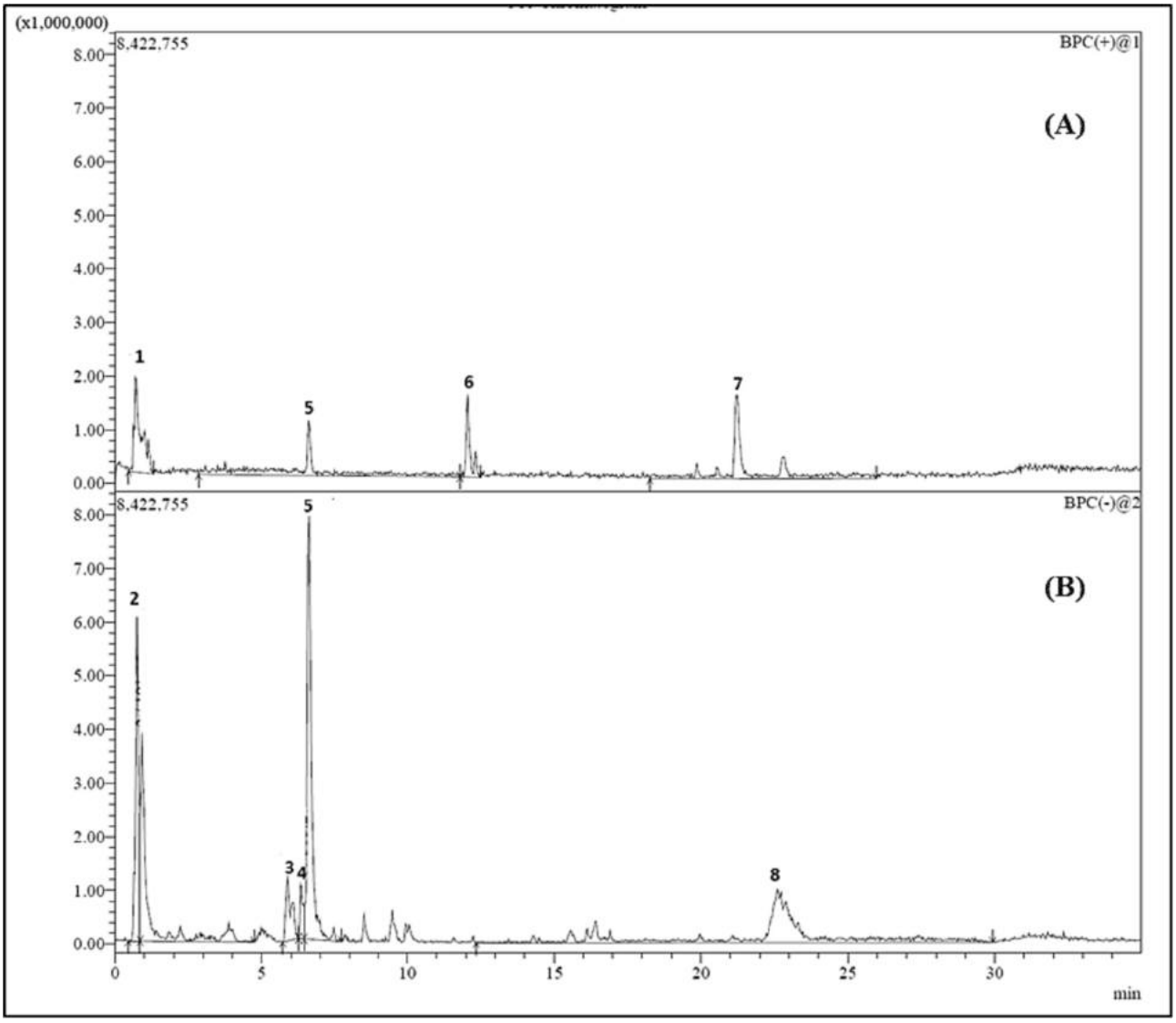

Fig. 2. UPLC-ESI-MS analysis of the negative and positive ion modes of 80 % methanol extract of *T. indica*.

2.6. In vivo assessment

Twenty adult male Wistar rats weighing 150–250 g were used in the present assay. The experimental procedures were inspected and approved by the Institutional Ethical Committee of Badr University in Cairo, Cairo, Egypt (BUC-IACUC-230507-25). It follows the guidelines of the US National Institute of Health. Rats were kept at a temperature of 25 ± 2 °C with a 2 h dark/light cycle during the experiment. Rats were fed a standard diet and permitted to access water freely [28]. A mixture of ketamine (35 mg/kg) and xylazine (5 mg/kg) were injected intraperitoneal in rats for anesthesia [29]. The back hair of rats was then shaved completely and disinfected with 70 % ethanol. A biopsy puncher was used to create a circular wound of 8 mm in diameter. The animals were assigned into five groups (4 animals/group), as listed in Table 1. Wounds in the treated groups were covered with the scaffolds and fixed with a sterile gauze while in the control group, the wounds were covered with sterile gauze only [30].

Wounds were imaged at day 0, 3, 7, 10 and 14, and the wound size was measured in the control and tested animals. Nanofibers scaffolds were replaced with new ones for animals after each measurement. Each wound was outlined on a translucent paper and wound closure percentage was determined and calculated *via* the following equation:

$$\text{Wound closure}\ (\%) = \frac{A_0 - A_{(N)}}{A_0} \times 100 \quad (1)$$

where, A_0 is the wound area at day 0 and $A_{(N)}$ is the wound area at day 3, 7, 10 or 14.

2.6.1. Histopathological evaluation

Tissue samples from the skin of the treated animals were fixed in buffered formalin. Then, dehydration in ascending grades of alcohol, clearing in xylene, and embedding in paraffin were carried out prior to sectioning. Sectioning of the tissue at 5 μm thickness and staining with hematoxylin and eosin stains (H&E) were performed [31].

2.7. Statistical analyses

Values are presented as means ± SDs of at least three independent experiments. Significant differences between groups were evaluated by one-way *ANOVA* followed by Tukey's multiple comparison tests. Differences between different groups were considered significant for p values <0.05.

Table 2
Metabolite profiling of 80 % methanol extract of *T. indica via* UPLC-ESI-MS/MS in the positive and negative ion modes.

Peak No.	Rt (min)	Compound Name	$[M-H]^-$/ $[M+H]^+$	MS/MS	UV λ_{max}	Molecular Formula	Class	Content %	Reference
1	0.72	Caffeic acid	−/181.20	–	265	$C_9H_8O_4$	Phenolic acid	9.71	18
2	0.92	Quinic acid	191.15	191 173, 127	274	$C_7H_{12}O_6$	Phenolic acid	13.18	19
3	5.87	Luteolin-7-*O*-hexoside	447.15	285, 241	250, 270	$C_{21}H_{20}O_{11}$	Flavonoid glycoside	3.71	28
4	6.33	Vicenin 1 (Apigenin 6-*C*- pentosyl-8-*C*- hexoside)	563.20	443, 383, 353 503,	230, 270	$C_{26}H_{28}O_{14}$	Flavonoid glycoside	1.29	20
5	6.61	Apigenin-O-hexoside	431.15/433.15	269, 225	270	$C_{21}H_{20}O_{10}$	Flavonoid glycoside	29.17	29
6	12.06	Eriodictyol	−/289.20	179, 151, 135, 107	285	$C_{15}H_{12}O_6$	Flavonoid	3.25	16, 30
7	21.21	Oleamide	−/282.25	97, 69, 149, 163	n.d.	$C_{18}H_{35}NO$	Fatty acid amide	11.43	28
8	22.61	Hydroxy-linoleic acid	277.35	251, 211, 195	277	$C_{18}H_{32}O_3$	Fatty acid	20.92	19

R_t: Retention time recorded for each compound; λmax: wavelength of maximum UV absorbance.

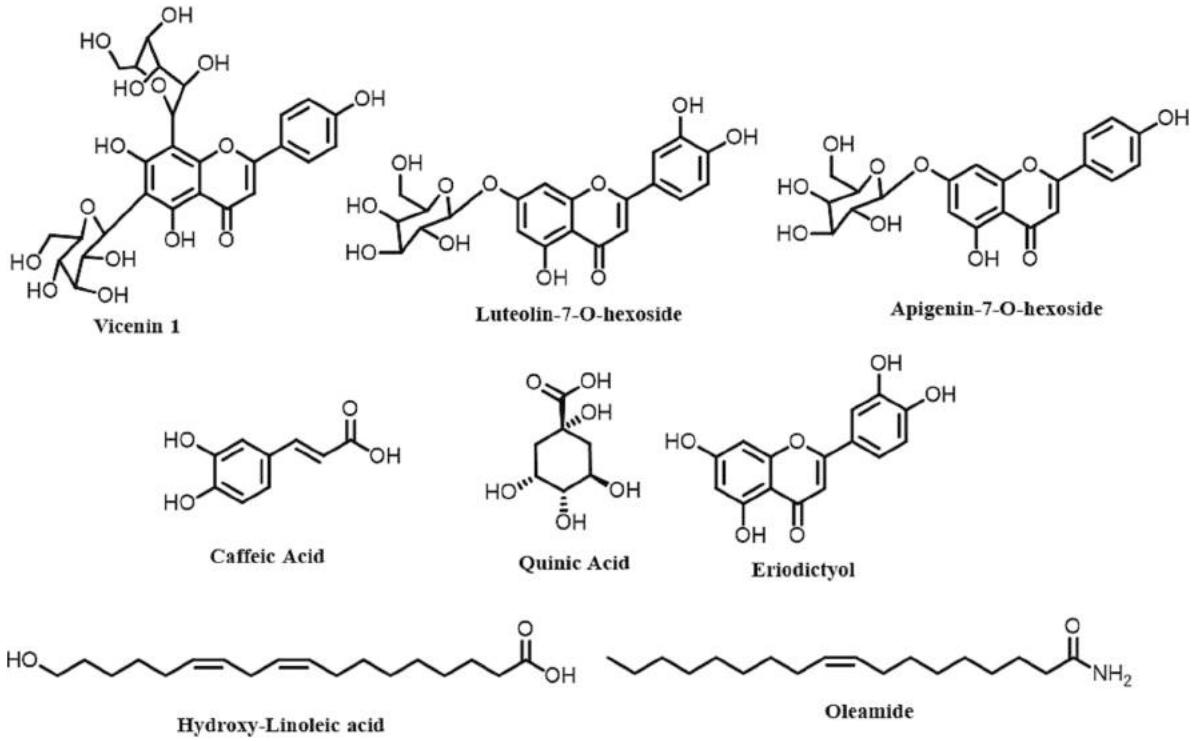

Fig. 3. Chemical structures of compounds identified in the 80 % methanol extract of *T. indica* using UPLC-ESI-MS/MS in the negative and positive ion modes.

3. Results and discussion

3.1. Preparation of nanofibrous scaffolds

3.1.1. Optimization of spinning conditions of PMMA/CA/PEO nanofibers

A series of various polymers at different volume ratios were blended to select the optimal composition that yield electrospun nanofibers of smooth surface, small diameter and beads-free nanofibers of homogenous distributions (*Tables S1 and S2, Supplementary Materials*). The spinning parameters were kept constant at applied voltage 20 kV, feed rate 1 mL/h, rotating speed 600 rpm, and a distance 12 cm. PMMA (10 %)/CA (2 % and 5 %) at various volume ratios (90:10, 80:20 and 60:40) were blended and electrospun using a flat collector to find out the optimal ratio. CA at 5 % was selected as the optimal concentration, because at lower concentration (*i.e.,* 2 %), more beaded and thinner nanofibers of increased weakness (*i.e.,* prone to break) were obtained. While PMMA:CA volume ratio (60:40) resulted in dense nanofibers of moderate diameter, lower number of beads and stronger nanofibers. Thereafter, the effect of addition of PEO at various concentrations (0.5, 1, 1.5, 2 and 3 %) on the overall morphology, diameter and characteristics of nanofibers comprised of PMMA (10 %)/CA (5 %) at volume ratio of 60:40 was studied.

PEO addition resulted in the formation of dense and continuous fibers, that have a homogenous aligned distribution. It is also noticed that the quality of PMMA/CA/PEO nanofibers was improved by increasing PEO concentration, where a beads-free, crosslinked, and aligned nanofibers were obtained at PEO concentrations of 1.5 % and 2 %. The surface morphology of electrospun nanofibers was investigated by SEM as depicted in Fig. 1. A round-shaped, non-woven, uniform, beads-free and well-oriented nanofibers of smooth surface were obtained at an average diameter of 300 ± 50 nm.

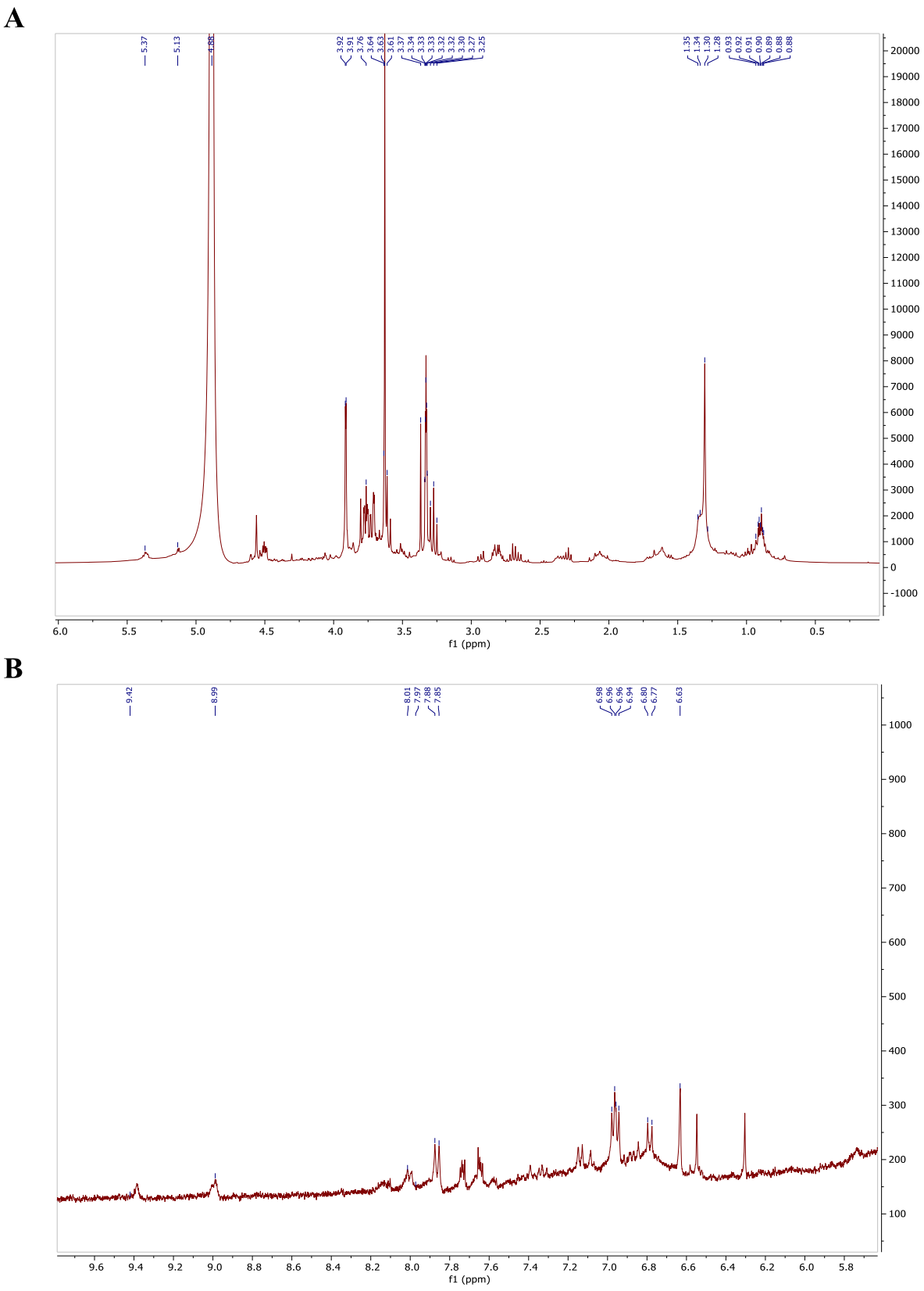

Fig. 4. ^{1}H NMR spectrum of 80 % methanol extract of *T. indica* A) spectrum region from δ 0 to 5.8, and B) spectrum region from δ 5.8 to 9.6 ppm.

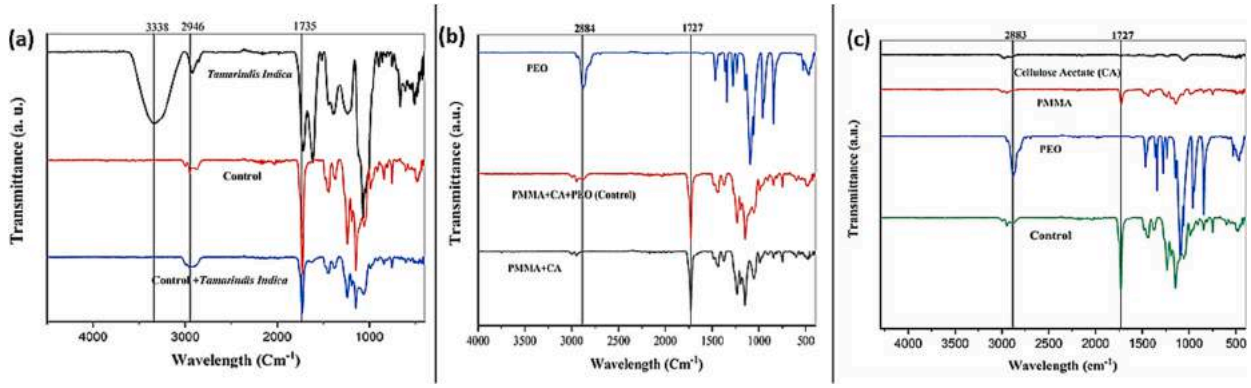

Fig. 5. FTIR of (a) Polymers: PMMA, CA, PEO and PMMA/CA/PEO control nanofiber without *T. indica* (plant extract), (b) optimized PMMA/CA nanofibers before and after addition of PEO *vs.* PEO polymer, and (c) *T. indica*, control nanofiber, PMMA/CA/PEO nanofiber-loaded *T. indica*.

3.1.2. Fabrication of electrospun T. indica loaded-PMMA/CA/PEO nanofibers

T. indica extract was incorporated into PMMA/CA/PEO nanofiber by blending the plant extract at various concentrations (0.01, 0.015 and 0.02 %) to polymer mixture solution at room temperature for 30 min before spinning. *T. indica*-loaded nanofibers were spun at voltage 20 kV, feed rate 1 mL/h, spinneret speed 100 rpm, spinneret width 15 mm, and distance 12 cm using the rotating drum at 600 rpm. The surface morphology and size of *T. indica*-loaded nanofibers were characterized by SEM. The average diameter of the control PMMA/CA/PEO nanofibers was 300 ± 150 nm, while the diameters of 0.01, 0.015 and 0.02 % *T. indica*-loaded PMMA/CA/PEO nanofibers were 300 ± 100 nm. Interestingly, *T. indica* extract has been encapsulated well in the nanofibers as indicated by smooth and uniform nanofibers except for slight beads/aggregates at nanofibers surface, which contain the highest concentration of *T indica*. Additionally, ATR-FTIR and XRD results revealed the encapsulation of *T. indica* into the nanofibers as confirmed by the disappearance of *T. indica* peaks in the spectrum of nanofibers.

3.2. Characterizations of PMMA/CA/PEO and T. indica loaded-PMMA/CA/PEO nanofibers

3.2.1. Plant extract (T. indica)

3.2.1.1. Total phenolics and total flavonoids. Polyphenolic compounds are among the most common secondary metabolites in medicinal plants. Besides, their medicinal and therapeutic efficacy plays an important role in development of natural treatments of various diseases [32,33]. The total phenolic content and total flavonoid content values were obtained from the calibration curve of gallic acid ($y = 0.0042\times - 0.0293$ with $R^2 = 0.9991$) and rutin ($y = 0.002\times - 0.0138$ with $R^2 = 0.998$) where x is the absorbance and y is the concentration of gallic acid and rutin solution (μg/mL), respectively (*Fig. S1, Supplementary Materials*). The results show that methanol extract of *T. indica* had total phenolics content of 22.94 ± 1.40 μg GA E/mg and total flavonoids content of 9.48 ± 0.44 μg RE/mg. The results indicated the methanol extract of *T. indica* leaves is rich in phenolic content compared to the flavonoid amount, in accordance with a previous report that showed a high percentage of phenolic compound in *T. indica* seeds and pericarp [34].

3.2.1.2. UPLC-ESI-MS analysis. Tentative metabolite identification was accomplished by comparing $[M-H]^-$ molecular ions in the negative ionisation mode with $[M+H]^+$ molecular ions in the positive ionisation mode, utilizing earlier published data and online databases (Fig. 2) [35–39]. It is worthy to highlight that; flavonoids are the major constituents in the methanol extract of *T. indica* leaves. As shown in Table 2, a total of eight metabolites were tentatively identified in *T. indica* including (phenolic acid: caffeic acid). Flavonoids were annotated as the major constituents including: luteolin-7-*O*-hexoside (3), vicenin 1 (4), apigenin-*O*-hexoside (5) and eriodictyol (6). Besides, miscellaneous compounds such as quinic acid (1) and fatty acid derivatives as oleamide (7) and hydroxy-linoleic acid (8) were identified. (Fig. 3) displays the structures of the phytoconstituents tentatively characterized in the 80 % methanol extract of leaves of *T. indica* using UPLC-ESI-MS.

3.2.1.3. ^1H NMR analysis of 80 % methanol extract of T. indica. The methanol extract of *T. indica* was dissolved in deuterated methanol (CD_3OD) for ^1H NMR (400 MHz) analysis. The observed peaks were resonated along with different chemical shifts at different regions. The observed peaks at δ 9.38 (s) and 8.98 (s) are characteristic hydroxyl protons of caffeic acid (Fig. 4). Besides, the presence of hydroxyl groups broad signal at δ 4.95 (br s) and 4.56 (s) indicated the presence of quinic acid [32]. The aromatic region of flavonoids shows different signals at δ 8.00 (*m*), 7.85 (d), 6.96 (*dd*) and 6.79 (d) ppm. The anomeric protons that appear at δ 5.36 and 5.13 ppm are characteristic for the presence of sugar moieties at the 6 and 8 positions of the flavonoids. The different chemical shifts of the remaining sugar protons resonated around δ of 3.76 to 1.76 ppm. Moreover, terminal -CH_3 groups at δ 0.92 (*m*) ppm and the long chain of -CH_2 groups at δ 1.32 ppm indicated the presence of fatty acid (Fig. 4) [40,41].

3.2.1.4. FTIR analysis of T. indica total methanol extract. FTIR was performed for identification of the typical peak values and the functional groups of *T. indica* total methanol extract (Fig. 5). The metabolic profiling of *T. indica* total methanol extract using FTIR indicates the existence of several metabolites as illustrated by the presence of different peaks corresponding to various functional groups (Fig. 5c). The presence of stretching vibrations at ν 3311.95 cm^{-1} is attributed to the O—H. Meanwhile, the peak at ν 2925.83 cm^{-1} could be assigned to the presence of = CH. Furthermore, the bands at ν 1439.28 and 1378.38 cm^{-1} are due to a bending vibration of O—H. Strong stretching C—O vibrations are observed at ν 1236.71, 1105.10 and 1008.99 cm^{-1}. Strong absorption at ν1719 cm^{-1} is attributed to the carbonyl stretching C═O. Additionally, the sharp and strong band corresponding to C-O-C group of sugar derivatives at ν 1067 cm^{-1} suggests the presence of glycosides. The absorption peak at νc1607 cm^{-1} is due to the C═C stretching for aromatic compounds [42,43]. The combination of MS, NMR and FTIR data provided insightful information on the bioactive compounds in the total methanol extract of *T. indica* leaves.

3.2.2. Electrospun T. indica loaded-PMMA/CA/PEO nanofibers

3.2.2.1. SEM investigation. As depicted in Table S2 (*Supplementary Materials*), SEM investigation of the fabricated nanofibers was helpful in optimizing the composition of PMMA/CA nanofibers. The results revealed that using the flat collector resulted in the formation of fibers

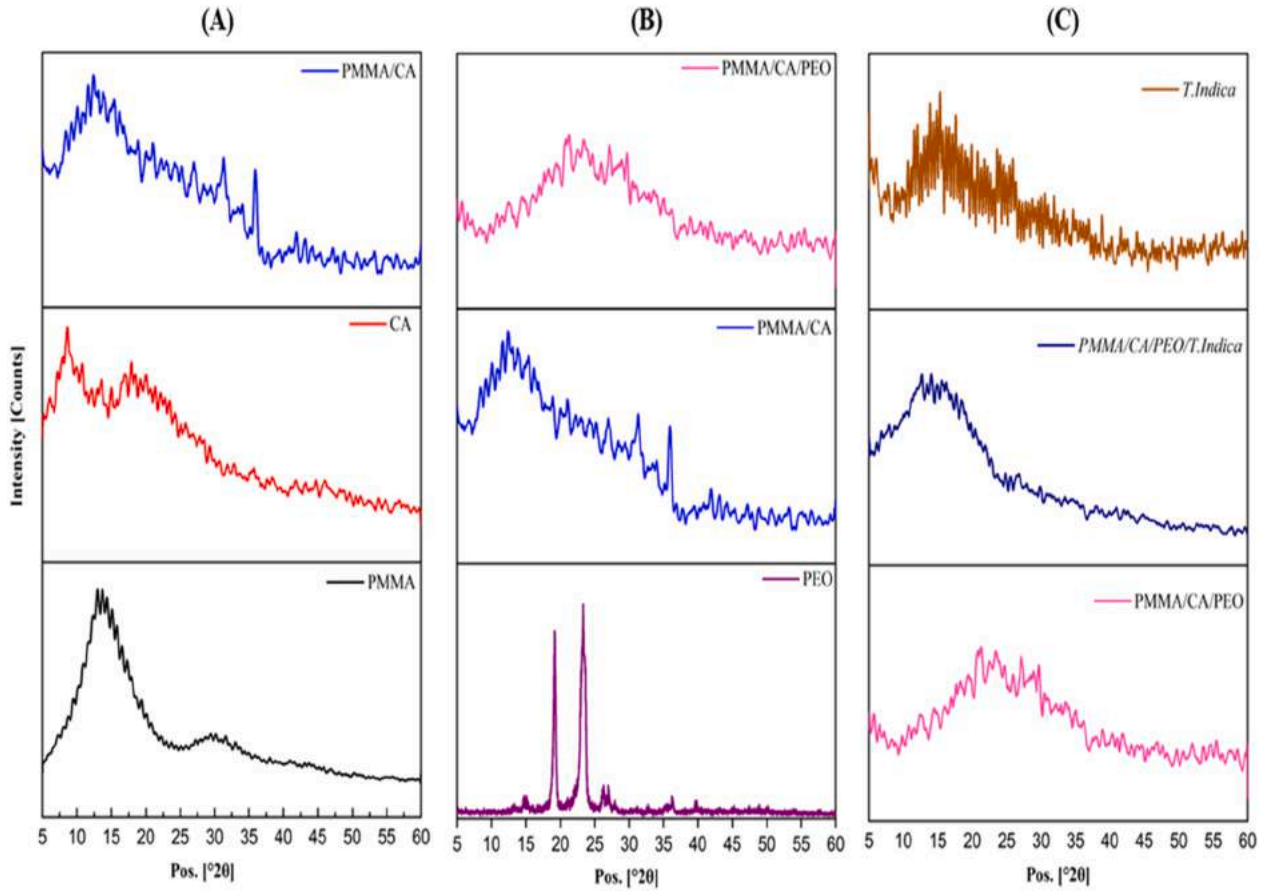

Fig. 6. XRD patterns of (A) Polymers: PMMA, CA, and PMMA/CA nanofibers (B) Optimized PMMA/CA nanofibers before and after addition of PEO (control) *vs.* PEO polymer, (C) *T. indica*, control nanofiber and *T. indica* loaded nanofiber.

that break at ends despite the homogenous distribution. On the contrary, utilizing the rotating collector might affect the molecular-level orientation within the fiber that in addition to the high shear and elongation forces results in the development of more aligned and less breakable nanofibers. Hence, the rotating collector was used in fabricating both PMMA/CA/PEO and *T. indica* loaded-PMMA/CA/PEO nanofibers. Moreover, utilizing lower CA concentration resulted in the formation of nanofibers of thinner diameter upon using both types of collectors (*i.e.*, rotating or flat collector). Upon addition of PEO to PMMA (10 %)/CA (2 %) at a volume ratio of (60:40), nanofibers revealed continuous and cross-linked nanofibers of small diameter, smooth surface and free of beads (Fig. 1). Moreover, all PEO concentrations (0.5–3 %) resulted in formation of continuous and bead-free nanofibers with variation in diameter and crosslinking degree. The fiber prepared using PEO at the concentration of 1.5 % resulted in the formation of nanofibers of optimal features. *T. indica* plant extract is then added to PMMA (10 %)/CA (2 %) as prepared at volume ratio (60:40)/PEO (1.5 %) at different concentrations. The resultant nanofibers display smooth surface, dense and continuous nanofibers (Fig. 1).

3.2.2.2. FTIR analysis of T. indica loaded-PMMA/CA/PEO nanofibers. ATR-FTIR spectra was acquired to assess the interaction between polymeric nanofiber blends upon electrospinning, and the successful loading of *T. indica* into the nanofibers. Fig. 5a depicts ATR-FTIR spectra of CA, PMMA and PEO polymers. CA spectrum shows -OH stretching band at ν 3660 cm^{-1}, -CH stretching vibrations at ν 2970 cm^{-1}. Furthermore, it is also characterized by carbonyl stretching band at ν 1730 cm^{-1}, ester stretching band at ν 1212 cm^{-1}, methyl bending vibrations at ν 1378 cm^{-1}, and ether stretching band at ν 1040 cm^{-1}. Moreover, PMMA exhibits characteristic carbonyl (C=O) band at ν 1730 cm^{-1} and C-O-C band at ν 1140 cm^{-1}, while two bands at ν 2995 cm^{-1} and 2950 cm^{-1} attribute to -CH sp^3 bond. On the other hand, FTIR spectra of PEO demonstrated characteristic absorption bands as follows: CH stretching vibrations at 2884 cm^{-1}, CH_2 scissoring at ν 1468 cm^{-1} and CH_2 asymmetric bending at ν 1342 cm^{-1}, while ν 1110 cm^{-1} absorption band corresponds to C-O-C stretching. Also, FTIR spectrum of PMMA/CA/PEO nanofibers (Fig. 5b) shows PMMA absorption peaks which might be attributed to the higher ratio and concentration of the PMMA polymer as the main scaffold. This also indicates the incorporation of PEO and CA polymer in the fiber composition. Additionally, ATR-FTIR spectrum of *T. indica*-loaded PMMA/CA/PEO nanofibers (Fig. 5c) shows the disappearance of *T. indica.* Main absorption bands at ν 3338, 2946, and 1735 cm^{-1}, which indicates the complete incorporation of the plant extract into the nanofiber, as was also confirmed by SEM.

3.2.2.3. X-ray diffraction of T. indica loaded-PMMA/CA/PEO nanofibers. Fig. 6 depicts the XRD patterns of fabricated nanofibers and the forming polymers. In Fig. 6A, the diffraction pattern of pure PMMA shows three patterns at 2θ ~13.4°, 30°, and a less intense peak at 2θ ~42° with 65 % crystallinity, while CA exhibits two less intense broad peaks at 2θ ~ 8.6° and 19°. Interestingly, the intense characteristic peak at 2θ ~13.4° of PMMA and those of CA almost vanished in PMMA/CA nanofiber pattern (blue, Fig. 6A), while a broad peak at 2θ ~ 6°-34° and a sharp peak at 2θ ~36° appeared instead. This could be attributed to the interaction between the PMMA and the CA polymers and the amorphous nature of the formed nanofibers. On the other hand, incorporating the highly crystalline PEO (~ 90 % crystallinity) into PMMA/CA nanofibers resulted in a broad peak at 2θ ~15°-35° with lower crystallinity (29.9 %) where the two most intense characteristic peaks of PEO at 2θ ~19° and 23° disappeared (Figs. 6A and B.). This indicates the interaction between

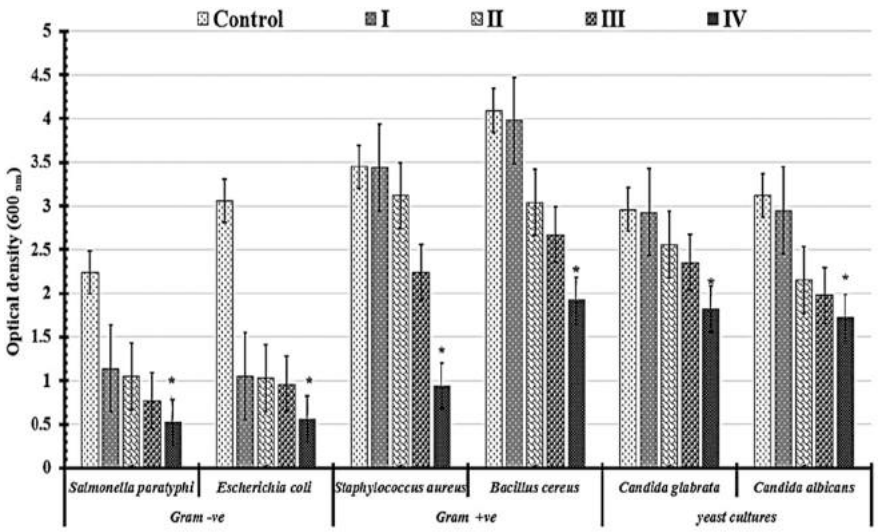

Fig. 7. Histogram illustrates the estimated antimicrobial activity of several nanofibers at various *Tamarindus indica* concentrations, including I = 0 %, II = 0.01 %, III = 0.015 %, and IV = 0.02 % (*w/v*) against multi-drug-resistant human pathogens. Significant differences ($p < 0.05$) are marked by the star symbol for major differences.

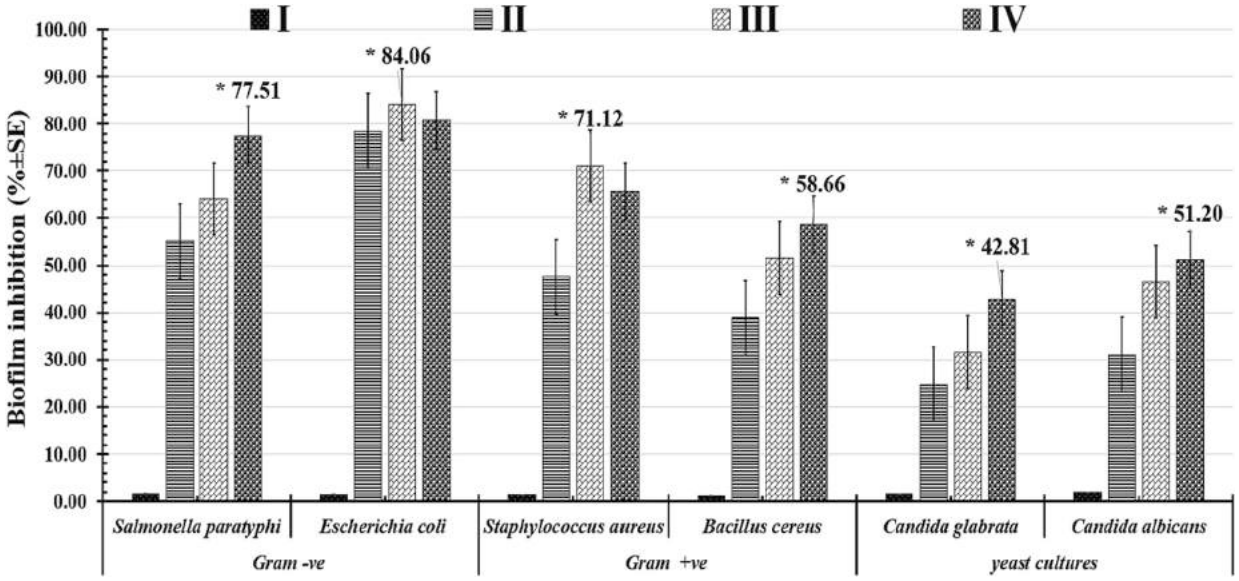

Fig. 8. Histogram illustrates the estimated biofilm inhibition percentage of several nanofibers at various *T. indica* concentrations, including *I* = 0 %, II = 0.01 %, III = 0.015 %, and IV = 0.02 %, (*w/v*) against multi-drug-resistant human pathogens by counting the number of colonies forming units generated *per* milliliter. Star symbols denote significant differences ($p < 0.05$) between each treatment and its control. Bars represent the standard error of the mean ($n = 3$).

the three polymers (*i.e.*, PMMA/CA/PEO) in the fabricated nanofibers. Additionally, *T. indica* plant extract diffraction pattern (Fig. 6C) reflects the amorphous nature of the plant extract with diffraction peaks at 2θ ~21° and 34°, showing the possibility of existence of other crystalline planes embedded in the diffractogram. However, *T. indica loaded-*/PMMA/CA/PEO nanofiber diffraction pattern reveals a shift in the peak position of PMMA/CA/PEO from 2θ ~15°-35° to 2θ ~9°-23° upon addition of plant extract with notable increase in the crystallinity to 42.23 % (Fig. 6C). This indicates the good interaction and loading of the *T. indica* extract into the PMMA/CA/PEO nanofibers.

3.3. Antimicrobial activity of T. indica loaded-PMMA/CA/PEO nanofibers

Basically, tamarind is considered as a significant source of polyphenols and their derivatives while, both Nerol and linalool were found in small amounts in some essential oils, might also have antimicrobial activity [44,45]. In our investigation, the antimicrobial effectiveness of four nanofiber formulations with varied *T. indica* concentrations (*I* = 0 %, II = 0.01 %, III = 0.015 % and IV = 0.02 %) was examined against several multi-drug resistant human pathogens (Fig. 7). Notably, all *T. indica* loaded-nanofibers formulations significantly inhibited the pathogen growth except yeast cells, which remained resistant. The antibacterial activity was higher at 0.02 % concentration of *T. indica* than that of 0.015 % nanofibers against *Escherichia coli* (0.56 ± 0.34), followed by *Salmonella Paratyphi* (0.52 ± 0.221), with a growth reduction of 81.69 ± 1.45 and 76.79 ± 2.36 %, respectively. Additionally, the 0.02 % nanofibers against *Staphylococcus aureus* (0.94 ± 0.213) inhibited microbial growth by 72.75 ± 0.89 %. Furthermore, nanofibers with 0.02 % *T. indica* had the lowest inhibitory activity against all tested yeast cells. When compared to the tested control, the growth of *Candida albicans* (1.72 ± 0.144) and *Candida glabrata* (1.82 ± 0.29) was reduced

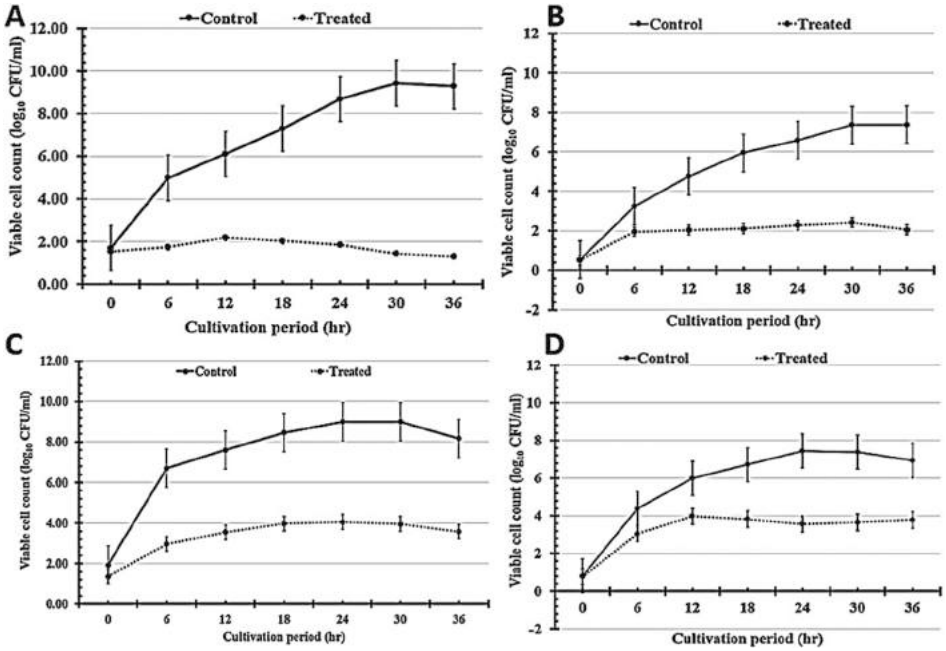

Fig. 9. Cultivation growth of human pathogens: *Escherichia coli* (A) and *Staphylococcus aureus* (B), treated with 0.015 % nanofibers as well as *Salmonella Paratyphi* (C) and *Candida albicans* (D) treated with the 0.02 % nanofibers *over* incubation periods to detect the time-kill kinetic analysis. At each time interval, each point indicates the relative viable count (log^{10} CFU/mL) of microbial cells.

Table 3
The percentages of HBF4 cell viability after incubation with free and NFs-loaded *T.indica.*

Dose (%)	% HBF4 cell viability	
	Free extract-treated cells	Loaded extract-treated cells
0	99.97 ± 0.084	100.0 ± 0.000
0.01	98.80 ± 0.73	99.15 ± 0.48
0.015	96.27 ± 2.20	95.80 ± 2.43
0.02	92.10 ± 1.63	93.48 ± 1.05
0.025	91.05 ± 1.01	93.45 ± 0.45
0.04	90.43 ± 1.81	91.49 ± 1.40

All values are expressed as mean ± SEM.

by 44.87 ± 2.45 and 38.51 ± 0.98 %, respectively.

The percentages of biofilm inhibition were calculated by counting the number of forming colonies of six different human pathogens exposed to all tested formulations, as shown in Fig. 8. The observed percentage of biofilm inhibition of the treated yeast cells was relatively low when compared to *Gram-negative* and *Gram-positive* bacteria. Both yeast strains exhibited the lowest percentage of biofilm reduction when treated with 0.02 % *T. indica*-loaded nanofibers, with an average of 51.19 ± 1.52 % for *Candida albicans* and 42.81 ± 1.12 % for *Candida glabrata*. In the case of *Gram-negative* bacteria, those tested with 0.015 %

Table 4
The percentages of wound healing of tested NFs free/loaded plant extract.

NF	% Wound healing	
	25.84 ± 1.15	
Dose (%)	Free extract-treated cells	Loaded extract-treated cells
0.01	34.43 ± 0.59	54.85 ± 1.04
0.015	43.96 ± 0.95	97.04 ± 1.81
0.02	81.89 ± 1.91	100.0 ± 0.00

All values are expressed as mean ± SEM.

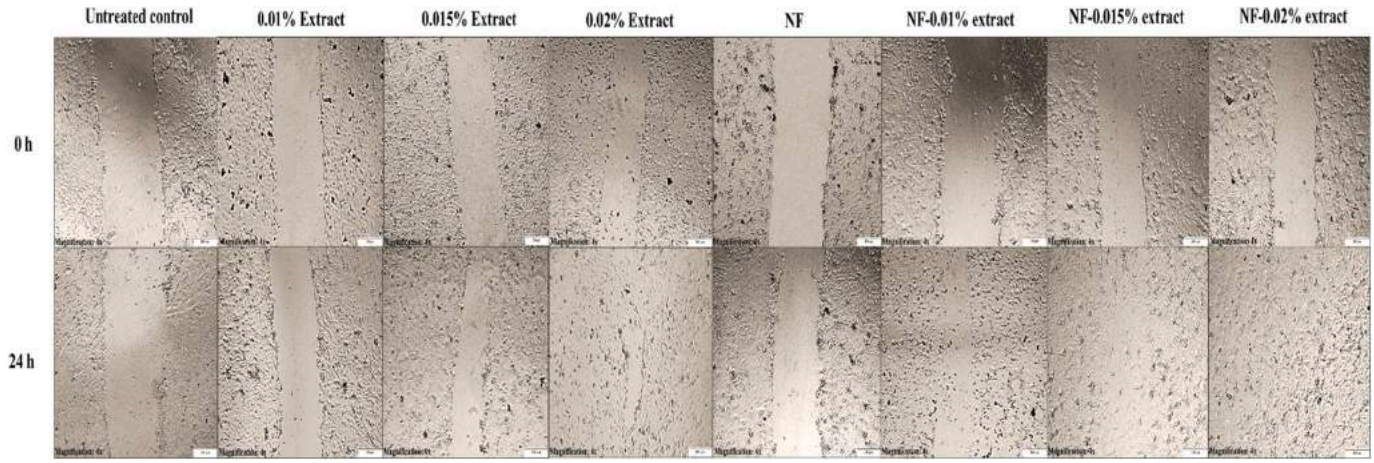

Fig. 10. Microscopic images of wound area (at 0 h and 24 h) in the untreated HBF4 cells (control) and treatment with 0.01 %, 0.015 %, 0.02 % *T. indica* extract and with nanofibers loaded with 0.01, 0.015, 0.02 % extract (Magnification 40 X; scale bar 200 μm).

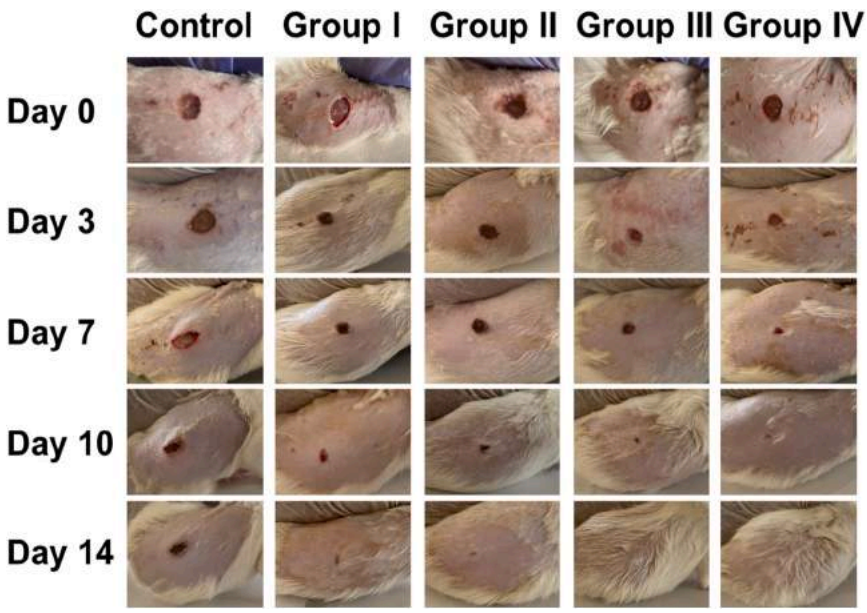

Fig. 11. Wounds were captured for each group during the 14 days of the experiment. In the control group, wounds were covered with sterile gauze, group I (nanofibers with no plant extract), group II (100 mg), group III (150 mg), group IV (200 mg).

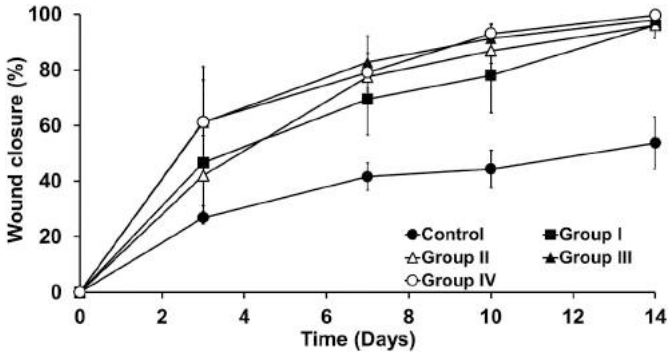

Fig. 12. Wound closure percentages at day 3, 7, 10 and 14 in the control and the treated groups.

and 0.02 % *T. indica*-loaded nanofibers show a significant difference. Because *E. coli* (84.06 ± 4.57 %) treated with 0.015 % *T. indica* loaded nanofibers had the highest percentage of biofilm reduction, *Salmonella Paratyphi* (77.51 ± 2.85) treated with 0.02 % nanofibers ranked second. While *Gram*-positive bacteria were treated with 0.015 % *T. indica*-loaded nanofibers, *Staphylococcus aureus* exhibited the highest percentage of biofilm reduction (71.12 ± 2.86 %). The impact that different doses of these compounds have on activity may be explained by the microbes' *Gram*, resistivity, and adaptability. Additionally, extra variables like the length of time it takes for the formulation to release its antimicrobial metabolites can affect them. Logically, lower doses of our active ingredients may be released more quickly than their bigger doses. Furthermore, although both dosages had an impact on human pathogens, the large doses took longer to start working than the low ones. Thus, the pathogens under investigation that showed the largest percentage of biofilm reduction (Fig. 8) were carefully evaluated using formulae of 150 or 200 mg, all the way through the time-Kill Kinetic Assay growth curve (Fig. 9).

In this study, Time-Kill kinetic assay was carried out *in vitro* against *Gram*-negative bacteria (*Salmonella Paratyphi* and *E. coli*), *Gram-positive* bacteria (*Staphylococcus aureus*), and *Candida albicans* using nanofibers loaded with 0.015 % and 0.02 % *T. indica,* as shown in Fig. 9. The period of incubation and the dose of tested nanofibers in contact with pathogen's cells influenced the viable cell count reduction. After 36 h of incubation, the relative viable count of *Escherichia coli* (Fig. 9A) and *Staphylococcus aureus* (Fig. 9B) at 0.015 % *T. indica*-loaded nanofibers decreased by 85.91 ± 3.12 %, and 72.19 ± 5.23 %, respectively. Additionally, the relative viable counts of *Salmonella Paratyphi* (Fig. 9C) and *Candida albicans* (Fig. 9D) lowered by 78.48 ± 3.09 % and 52.13 ± 2.12 %, respectively, after 24 h of incubation with 0.02 % *T. indica*-loaded nanofibers.

The bactericidal time (99.9 % killing) is determined to be the critical interval for tested nanofibers that would lower the initial inoculum by >3 Log^{10} CFU/mL. Herein, the bactericidal time for both 0.015 % and 0.02 % *T. indica*-loaded nanofibers was selected after 72 h of cultivation. Finally, it was observed that the nanofibers containing 0.02 % of *T. indica* was found to be more effective against *Gram-negative* bacteria than *Gram-positive* bacteria and yeast cells. *T. indica* has previously been identified as a highly promising antimicrobial agent due to its inhibitory effects on pathogens attributed to bacterial cell wall damage and significant modifications in gene expression [44–46]. Accordingly, the composition had a significant antimicrobial activity and thus could provide an eco-friendly antimicrobial agent to suppress the growth of a wide range of human pathogens.

The extracts of *T. indica* contain phenolic antioxidants, campesterol, b-amyrin, and fatty acids (palmitic acid, eicosanoic acid) as their active chemical constituents or secondary bioactive metabolites [44]. It has been demonstrated that these bioactive metabolites possess antimicrobial effects through several antimicrobial pathways. There are many antimicrobial mechanism theories that were described previously. The effects of these natural metabolites blocked the development of microbial biofilms and prevented cell adhesion, which is the process by which cells interact and adhere to one another *via* specific molecules on the cell surface. Moreover, these metabolites' bioactivities are connected to polyphenol interactions with biomolecules such as proteins, lipids, and carbohydrates, causing changes in the target bacteria's cell permeability and ultimately destroying their cell walls [19]. These metabolites have the ability to restrict the expression of microbial genes by binding to protein molecules (amino acids interactions) and regulatory enzymes. Utilizing tamarind extracts could reduce the duration, dosage, and toxicity hazards related to using antibiotics. It can also reduce the chance of resistant strains resurfacing [47]. However, the mechanisms by which the extracted metabolites influence the behavior of

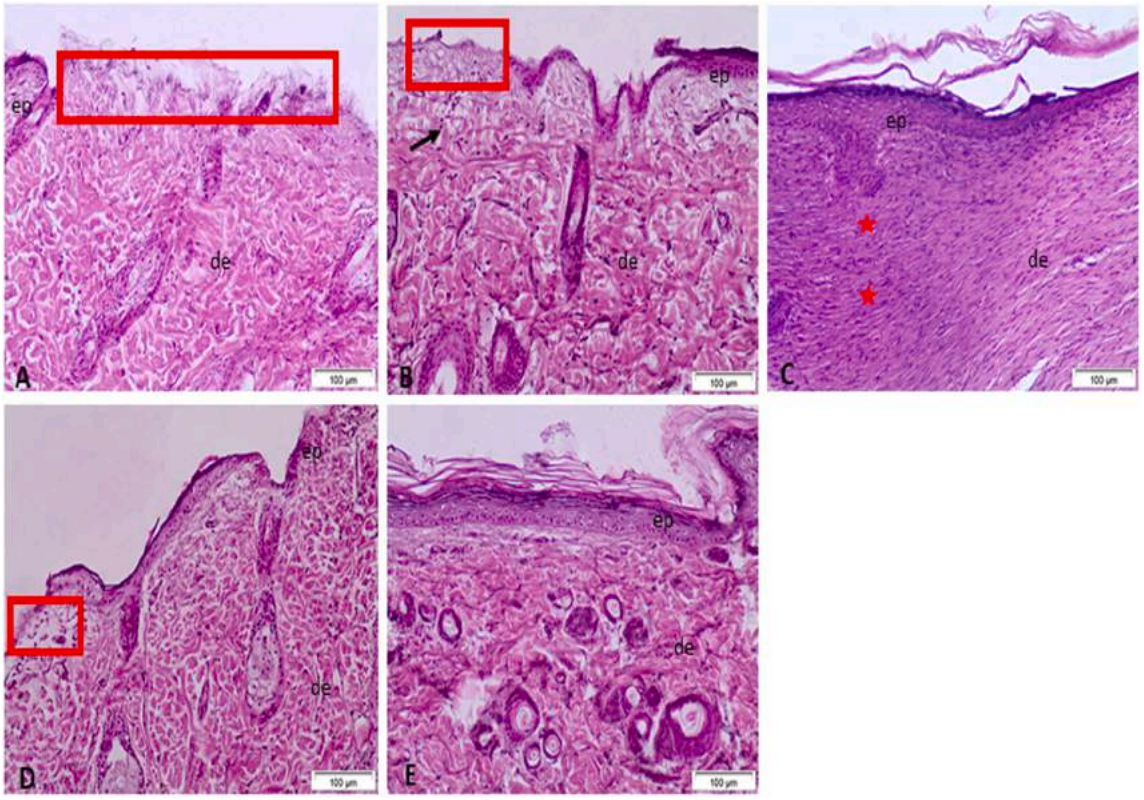

Fig. 13. Representative micrograph of the skin stained by H&E stain. A) Control positive group showing large ulcer (red rectangle) with necrosis with inflammatory cell infiltrations. B) Group (I): the group of nanofibers without drug showing ulcer (red rectangle), inflammatory cells (black arrow). C) Group (II) showing excessive granulation tissue in the dermis. D) Group (III) showing small ulcer (red rectangle). E) Group (IV) showing normal skin epidermis (ep) and dermis (de). Scale bar = 100 µm. (For interpretation of the references to colour in this figure legend, the reader is referred to the web version of this article.)

microorganisms remain unclear, particularly regarding their impact on the expression of genes associated with human pathogens.

3.4. In vitro bio-evaluation

3.4.1. In vitro cell viability

After incubating HBF4 with serial concentrations of free or loaded form of extract, all tested extracts exhibited high safety on the growth of HBF4 in a dose-dependent manner. The estimated safe doses (EC_{100}) of the two forms were 0.91 ± 0.08 % and 0.97 ± 0.03 %, respectively (Table 3). Furthermore, the calculated IC_{50} values of free and loaded extract were 3.89 ± 0.17 % and 3.94 ± 0.054 %, respectively. (Table 3). Furthermore, the calculated IC_{50} values of free and loaded extract were 3.89 ± 0.17 % and 3.94 ± 0.054 %, respectively.

3.4.2. In vitro scratch wound assay

As illustrated in Fig. 10 and Table 4, 0.01 %, 0.015 % and 0.02 % of free extract can enhance healing of the wound in the scratched HBF4 cells by 34.43 %, 43.96 % and 81.89 %, respectively. Meanwhile, the loading of extract in the nanofibers significantly increased its healing activity to 54.85 %, 98.04 % and 100 %, respectively. Only in nanofibers loaded with 0.02 % extract-treated wells, the wound was completely healed. In this study, the employed nano-fibrous material is made up of poly(methyl methacrylate) (PMMA), poly(ethylene oxide) (PEO), and cellulose acetate (CA), all of which have demonstrated strong efficacy in promoting the wound-healing properties of various substances [48]. Previous study demonstrated that PMMA enhanced wound closure *via* its potential as tissue adhesive agent [49] and self-healing agent [48]. Furthermore, PEO promoted the electrospinning of the used polymers and decreased the use of organic solvents with enhancing cell adhesion [50]. CA has high biocompatibility and exhibits promising potential for regulating drug release making it a strong candidate for drug delivery. However, it has not enough bioactivity to improve efficient skin repair [51,52]. Accordingly, the loaded *T. indica* exhibited higher migration activity than its corresponding unloaded extract (Fig. 10, Table 4).

3.5. In vivo assessment

3.5.1. Wound healing rate analysis

T. indica has been used to treat wounds in folk medicine in Africa that is attributed to its powerful antioxidant and antibacterial properties [47]. A wound model of 20 adult male rats was examined in this study. Wounds were captured at specific time intervals (day 0, 3, 7, 10 and 14) as shown in Fig. 11. Treated groups displayed a significant high wound closure percentage compared to the control group. Group III and group IV demonstrated the highest wound closure percentage owing to the high concentration of the plant extract. On day 3, groups III and IV showed an undoubtedly high wound closure percentage (*ca.* 61 %) compared to other groups. This pattern continued throughout the whole experiment. In each time interval, the wound closure percentage was determined and compared with that measured on day 0 (Fig. 12). On day 14, a complete wound closure was observed in group IV (*ca.* 99.7 %), though the wound closure percentage in the control group was 48.4 %.

Histopathological examination of the skin of rats in positive control group revealed the necrosis of the epithelial lining and ulceration infiltration of inflammatory cells in both epidermis and dermis (Fig. 13A). The group of rats treated with the nanofiber (Group I) showed areas of ulceration and infiltration with inflammatory cells but less than control positive group. In addition, hemorrhages in the dermis were noticed (Fig. 13B). Examination of group (II) revealed regeneration of the epithelium with no ulcers and excessive granulation tissue in the dermis (Fig. 13C). Examination of group (III) showed small areas of

ulceration (Fig. 13D). Histopathological examination of group (IV) revealed normal appearance of skin epidermis and dermis with normal skin adnexa (Fig. 13E).

4. Conclusions

In conclusion, biocompatible electrospun *Tamarindus indica* (*T. indica*)-loaded crosslinked poly (methyl methacrylate) (PMMA)/ cellulose acetate (CA)/poly(ethylene oxide) (PEO) nanofiber mats were designed and fabricated for wound healing applications. The spinning conditions were optimized to PMMA (10 %)/CA (5 %) at volume ratio (60:40) at an optimized voltage 20 Kv, collector distance 12 cm, and spinning feed rate 1 mL/h. The fabricated *T. indica*-loaded nanofibers exhibited desirable morphological properties with higher compatibility. Additionally, the fabricated nanofibers exhibited antimicrobial behavior with low cytotoxicity, *in vitro* with an increased healing activity of *HBF4* cells with the loaded nanofibers compared to the plant extract activity alone. *In vivo*, loaded fabricated nanofibers resulted in superior wound healing efficiency compared to the control untreated animals and animals treated with the plant extract. Therefore, the fabricated nanofibers loaded with potent phytochemicals could be employed as an effective biocompatible and eco-friendly antimicrobial biomaterials and wound healing/ wound dressing composites.

Ethics approval and consent to participate

Not applicable.

Consent of publications

Available publications for all data and figures

Funding

No funding was received for conducting this work.

Ethical statement

In-vivo experiments were carried out according to Helsinki World Medical Association's Declaration: Ethical Medical Research Principles Involving Human Subjects. *In vivo* experiments were done as Institutional Ethical Committee of Badr University in Cairo, Cairo, Egypt (BUC-IACUC-230507-25.

CRediT authorship contribution statement

Shaimaa S. Goher: Writing – original draft, Methodology. **Shaza H. Aly:** Resources, Methodology, Formal analysis. **Marwa M. Abu-Serie:** Validation, Methodology, Formal analysis. **Shahira H. EL-Moslamy:** Software, Resources, Methodology, Data curation, Conceptualization. **Ayat A. Allam:** Methodology, Investigation. **Nadeen H. Diab:** Methodology, Investigation. **Khaled M.A. Hassanein:** Methodology, Investigation, Formal analysis. **Rana A. Eissa:** Methodology, Investigation. **Noura G. Eissa:** Methodology, Investigation, Formal analysis, Data curation. **Mahmoud Elsabahy:** Writing – review & editing, Writing – original draft, Supervision, Resources, Funding acquisition. **Elbadawy A. Kamoun:** Writing – review & editing, Writing – original draft, Supervision, Funding acquisition.

Declaration of competing interest

The authors declare no competing of interests.

Data availability

All data are available.

Appendix A. Supplementary data

Supplementary data to this article can be found online at https://doi.org/10.1016/j.ijbiomac.2023.128793.

References

[1] S. Chen, B. Liu, M.A. Carlson, A.F. Gombart, D.A. Reilly, J. Xie, Recent advances in electrospun nanofibers for wound healing, Nanomedicine (Lond.) 12 (2017) 1335–1352, https://doi.org/10.2217/nnm-2017-0017.
[2] S. Guo, L.A. Dipietro, Factors affecting wound healing, J. Dent. Res. 89 (2010) 219–229, https://doi.org/10.1177/0022034509359125.
[3] M. Zare, A. Bigham, M. Zare, H. Luo, E. Rezvani Ghomi, S. Ramakrishna, pHEMA: An Overview for Biomedical Applications., Int. J. Mol. Sci. 22 (2021), https://doi.org/10.3390/ijms22126376.
[4] I. Alghoraibi, S. Alomari, in: A. Barhoum, M. Bechelany, A.S.H. Makhlouf (Eds.), Different Methods for Nanofiber Design and Fabrication BT-Handbook of Nanofibers, Springer International Publishing, Cham, 2019, pp. 79–124, https://doi.org/10.1007/978-3-319-53655-2_11.
[5] M.I. El Gohary, B.M.A. El Hady, A.A. Al Saeed, A.M.I. El Rashedi, S.I. Saleh, Controlling the Features of Electrospun Nanofibers, 2018.
[6] S.M.S. Shahriar, J. Mondal, M.N. Hasan, V. Revuri, D.Y. Lee, Y.-K. Lee, Electrospinning nanofibers for therapeutics delivery, Nanomater. (Basel, Switzerland) 9 (2019), https://doi.org/10.3390/nano9040532.
[7] A. Ahmadian, A. Shafiee, N. Aliahmad, M. Agarwal, Overview of Nano-Fiber Mats fabrication via electrospinning and morphology analysis, Textiles 1 (2021) 206–226, https://doi.org/10.3390/textiles1020010.
[8] J. Fang, H. Niu, T. Lin, X. Wang, Applications of electrospun nanofibers, Chin. Sci. Bull. 53 (2008) 2265–2286, https://doi.org/10.1007/s11434-008-0319-0.
[9] D. Han, P.-I. Gouma, Electrospun bioscaffolds that mimic the topology of extracellular matrix, Nanomedicine Nanotechnology. Biol. Med. 2 (2006) 37–41, https://doi.org/10.1016/j.nano.2006.01.002.
[10] S. Kajdič, O. Planinšek, M. Gašperlin, P. Kocbek, Electrospun nanofibers for customized drug-delivery systems, J. Drug Deliv. Sci. Technol. 51 (2019) 672–681, https://doi.org/10.1016/j.jddst.2019.03.038.
[11] X. Feng, J. Li, X. Zhang, T. Liu, J. Ding, X. Chen, Electrospun polymer micro/ nanofibers as pharmaceutical repositories for healthcare, J. Control. Release 302 (2019) 19–41, https://doi.org/10.1016/j.jconrel.2019.03.020.
[12] Y. Hussein, E.M. El-Fakharany, E.A. Kamoun, S.A. Loutfy, R. Amin, T.H. Taha, S. A. Salim, M.S. Amer, Electrospun PVA/hyaluronic acid/L-arginine nanofibers for wound healing applications: nanofibers optimization and in vitro bioevaluation, Int. J. Biol. Macromol. 164 (1) (2020) 667–676.
[13] S.A. Salim, S.A. Loutfy, E.M. El-Fakharany, T.H. Taha, Y. Hussien, E.A. Kamoun, Influence of chitosan and hydroxyapatite incorporation on properties of electrospun PVA/HA nanofibrous mats for bone tissue regeneration: nanofibers optimization and in-vitro assessment, J. Drug Deliv. Sci. Technol. 62 (2021), 102417, https://doi.org/10.1016/j.jddst.2021.102417.
[14] U. Ali, K.J.B.A. Karim, N.A. Buang, A review of the properties and Applications of poly (methyl methacrylate) (PMMA), Polym. Rev. 55 (2015) 678–705, https://doi.org/10.1080/15583724.2015.1031377.
[15] S.O. Han, J.H. Youk, K.D. Min, Y.O. Kang, W.H. Park, Electrospinning of cellulose acetate nanofibers using a mixed solvent of acetic acid/water: effects of solvent composition on the FIBER diameter, Mater. Lett. 62 (2008) 759–762.
[16] L. Shuiping, T. Lianjiang, H. Weili, L. Xiaoqiang, C. Yanmo, Cellulose acetate nanofibers with photochromic property: fabrication and characterization, Mater. Lett. 64 (2010) 2427–2430, https://doi.org/10.1016/j.matlet.2010.08.018.
[17] R. Konwarh, N. Karak, M. Misra, Electrospun cellulose acetate nanofibers: the present status and gamut of biotechnological applications, Biotechnol. Adv. 31 (2013) 421–437, https://doi.org/10.1016/j.biotechadv.2013.01.002.
[18] P. Kuru, Tamarindus indica and its health related effects, Asian Pac. J. Trop. Biomed. 4 (2014) 676–681, https://doi.org/https://doi.org/10.12980/APJTB.4.2014APJTB-2014-0173.
[19] K.O. Fagbemi, D.A. Aina, M.O. Adeoye-Isijola, K.K. Naidoo, R.M. Coopoosamy, O. O. Olajuyigbe, Bioactive compounds, antibacterial and antioxidant activities of methanol extract of Tamarindus indica Linn, Sci. Rep. 12 (2022) 9432, https://doi.org/10.1038/s41598-022-13716-x.
[20] N. Razali, S. Mat-Junit, A.F. Abdul-Muthalib, S. Subramaniam, A. Abdul-Aziz, Effects of various solvents on the extraction of antioxidant phenolics from the leaves, seeds, veins and skins of Tamarindus indica L, Food Chem. 131 (2012) 441–448, https://doi.org/10.1016/j.foodchem.2011.09.001.
[21] H.A. Fathi, A. Abdelkader, M.S. AbdelKarim, A.A. Abdelaziz, M.A. El-Mokhtar, A. Allam, G. Fetih, M. El Badry, M. Elsabahy, Electrospun vancomycin-loaded nanofibers for management of methicillin-resistant Staphylococcus aureus-induced skin infections, Int. J. Pharm. 586 (2020), 119620, https://doi.org/10.1016/j.ijpharm.2020.119620.
[22] R.A. Eissa, H.A. Saafan, A.E. Ali, K.M. Ibrahim, N.G. Eissa, M.A. Hamad, C. Pang, H. Guo, H. Gao, M. Elsabahy, K.L. Wooley, Design of nanoconstructs that exhibit enhanced hemostatic efficiency and bioabsorbability, Nanoscale 14 (2022) 10738–10749, https://doi.org/10.1039/d2nr02043b.
[23] M. Elsabahy, M.A. Hamad, Design and preclinical evaluation of chitosan/kaolin nanocomposites with enhanced hemostatic efficiency, Mar. Drugs 19 (2021), https://doi.org/10.3390/md19020050.
[24] M. Elsabahy, M. Zhang, S.-M. Gan, K.C. Waldron, J.-C. Leroux, Synthesis and enzymatic stability of PEGylated oligonucleotide duplexes and their self-assemblies

with polyamidoamine dendrimers, Soft Matter 4 (2008) 294–302, https://doi.org/10.1039/B714221H.
[25] L. Tan, J. Hu, H. Huang, J. Han, H. Hu, Study of multi-functional electrospun composite nanofibrous mats for smart wound healing, Int. J. Biol. Macromol. 79 (2015) 469–476, https://doi.org/10.1016/j.ijbiomac.2015.05.014.
[26] L. Zhou, L. Cai, H. Ruan, L. Zhang, J. Wang, H. Jiang, Y. Wu, S. Feng, J. Chen, Electrospun chitosan oligosaccharide/polycaprolactone nanofibers loaded with wound-healing compounds of Rutin and Quercetin as antibacterial dressings, Inter. J. Biolog. Macrmol. 183 (2021) 1145–1154.
[27] Y. Song, L. Cai, Z. Tian, Y. Wu, J. Chen, Phytochemical curcumin-Coformulated, silver-decorated melanin-like Polydopamine/mesoporous silica composites with improved antibacterial and chemotherapeutic effects against drug-resistant Cancer cells, ACS Omega 5 (25) (2020) 15083–15094.
[28] A.I. Mekkawy, M.A. El-Mokhtar, N.A. Nafady, N. Yousef, M.A. Hamad, S.M. El-Shanawany, E.H. Ibrahim, M. Elsabahy, In vitro and in vivo evaluation of biologically synthesized silver nanoparticles for topical applications: effect of surface coating and loading into hydrogels, Int. J. Nanomedicine 12 (2017) 759–777, https://doi.org/10.2147/IJN.S124294.
[29] S. Selvaraj, N.N. Fathima, Fenugreek incorporated silk fibroin nanofibers—a potential antioxidant scaffold for enhanced wound healing, ACS Appl. Mater. Interfaces 9 (2017) 5916–5926, https://doi.org/10.1021/acsami.6b16306.
[30] O.E. Fayemi, A.C. Ekennia, L. Katata-Seru, A.P. Ebokaiwe, O.M. Ijomone, D. C. Onwudiwe, E.E. Ebenso, Antimicrobial and wound healing properties of Polyacrylonitrile-Moringa extract nanofibers, ACS Omega 3 (2018) 4791–4797, https://doi.org/10.1021/acsomega.7b01981.
[31] D.R. Banchroft, J.D. Stevens, A. Turner, Theory and Practice of Histological Techniques, Fourth, Churchil Livingstone, New York, 1996.
[32] S.H. Aly, A.M. Elissawy, A.M. Fayez, O.A. Eldahshan, M.A. Elshanawany, A.N. B. Singab, Neuroprotective effects of Sophora secundiflora, Sophora tomentosa leaves and formononetin on scopolamine-induced dementia, Nat. Prod. Res. 35 (2021) 5848–5852, https://doi.org/10.1080/14786419.2020.1795853.
[33] S.H. Aly, A.M. Elissawy, O.A. Eldahshan, M.A. Elshanawany, T. Efferth, A.N. B. Singab, The pharmacology of the genus Sophora (Fabaceae): An updated review, Phytomedicine 64 (2019), 153070.
[34] Y. Sudjaroen, R. Haubner, G. Würtele, W.E. Hull, G. Erben, B. Spiegelhalder, S. Changbumrung, H. Bartsch, R.W. Owen, Isolation and structure elucidation of phenolic antioxidants from tamarind (Tamarindus indica L.) seeds and pericarp, Food Chem. Toxicol. 43 (11) (2005) 1673–1682.
[35] J.C. Escalona-Arranz, R. Pérez-Rosés, I.L. Jimenez, J. Rodríguez-Amado, H. Argota-Coello, J. Cañizares-Lay, H.J. Morris-Quevedo, G. Sierra-González, Chemical CONSTITUENTS of Tamarindus indica L. leaves, Rev. Cuba. Química. (2010) 65–71.
[36] I.M. Ayoub, M. Korinek, M. El-Shazly, B. Wetterauer, H.A. El-Beshbishy, T.-L. Hwang, B.-H. Chen, F.-R. Chang, M. Wink, A.N.B. Singab, F.S. Youssef, Anti-allergic, anti-inflammatory, and anti-hyperglycemic activity of Chasmanthe aethiopica leaf extract and its profiling using LC/MS and GLC/MS, Plants 10 (2021), https://doi.org/10.3390/plants10061118.
[37] Z. Benayad, C. Gómez-Cordovés, N.E. Es-Safi, Characterization of flavonoid glycosides from fenugreek (Trigonella foenum-graecum) crude seeds by HPLC-DAD-ESI/MS analysis, Int. J. Mol. Sci. 15 (2014) 20668–20685, https://doi.org/10.3390/ijms151120668.
[38] E. De Caluwé, K. Halamová, P. Van Damme, Tamarind (*Tamarindus indica* L.): a review of traditional uses, phytochemistry and pharmacology, African Nat. Plant Prod. New Discov. Challenges Chem. Qual., American Chemical Society (2009) 5–85, https://doi.org/10.1021/bk-2009-1021.ch005.
[39] M.A. Farag, A. Porzel, L.A. Wessjohann, Comparative metabolite profiling and fingerprinting of medicinal licorice roots using a multiplex approach of GC-MS, LC-MS and 1D NMR techniques, Phytochemistry 76 (2012) 60–72, https://doi.org/10.1016/j.phytochem.2011.12.010.
[40] A. Dawod, S.I. Fathalla, A. ElKhatam, N. Osman, N.I. Sheraiba, M.A. Hammad, H. R. El-Seedi, A.A. Shehata, A. Anis, UPLC-QToF Nanospray MS and NMR Analysis of *Ficus sycomorus* Stem Bark and its Effects on Rabbit, Processes, 2021.
[41] S. El-mekkawy, A.A. Shahat, A.S. Alqahtani, M.S. Alsaid, M.A.O. Abdelfattah, R. Ullah, M.A. Emam, A. Yasri, M. Sobeh, A polyphenols-rich extract from Moricandia sinaica boiss. exhibits analgesic, anti-inflammatory and antipyretic activities in vivo, Molecules 25 (2020).
[42] A. Fatima, S. Yasir, M.S. Khan, S. Manan, M.W. Ullah, M. Ul-Islam, Plant Extract-Loaded Bacterial Cellulose Composite Membrane for Potential Biomedical Applications, 2021.
[43] M. Adeli-Sardou, M.M. Yaghoobi, M. Torkzadeh-Mahani, M. Dodel, Controlled release of lawsone from polycaprolactone/gelatin electrospun nano fibers for skin tissue regeneration, Int. J. Biol. Macromol. 124 (2019) 478–491, https://doi.org/10.1016/j.ijbiomac.2018.11.237.
[44] W. Kamil, H. Haidar Ahm, A. Ibrahim Ha, T.-E. Elmissbah, H. Dahlawi, Antimicrobial activity of tamarind seeds extract on Pseudomonas aeruginosa biofilm forming isolates, Int. J. Pharmacol. 18 (2022) 618–622, https://doi.org/10.3923/ijp.2022.618.622.
[45] C. Gupta, D. Prakash, S. Gupta, Studies on the antimicrobial activity of tamarind (Tamarindus indica) and its potential as food bio-preservative, Int. Food Res. J. 21 (2014) 2437–2441.
[46] U.U. Nwodo, G.E. Obiiyeke, V.N. Chigor, A.I. Okoh, Assessment of Tamarindus indica extracts for antibacterial activity, Int. J. Mol. Sci. 12 (2011) 6385–6396, https://doi.org/10.3390/ijms12106385.
[47] S.S. Bhadoriya, A. Ganeshpurkar, J. Narwaria, G. Rai, A.P. Jain, Tamarindus indica: extent of explored potential, Pharmacogn. Rev. 5 (2011) 73–81, https://doi.org/10.4103/0973-7847.79102.
[48] M. Peñas-Caballero, E. Chemello, A.M. Grande, M. Hernández Santana, R. Verdejo, M.A. Lopez-Manchado, Poly(methyl methacrylate) as healing agent for carbon fibre reinforced epoxy composites, Polymers 15 (2023) 1114.
[49] R. Suzuki, Y. Kuroyanagi, Safety and utility of a PMMA-based tissue adhesive for closure of surgical incision wounds, J. Biomater. Sci. Polym. Ed. 24 (3) (2023) 287–300.
[50] H. Nosrati, M. Khodaei, M. Banitalebi-Dehkordi, M. Alizadeh, S. Asadpour, E. Sharifi, J. Ai, M. Soleimannejad, Preparation and characterization of poly (ethylene oxide)/zinc oxide nanofibrous scaffold for chronic wound healing applications, Polim. Med. 50 (1) (2020) 41–51.
[51] A. Akturk, Enrichment of cellulose acetate nanofibrous scaffolds with retinyl palmitate and clove essential oil for wound healing applications, ACS Omega. 8 (6) (2023) 5553–5560.
[52] Y. Fan, Y. Zhi, M. He, B. Ahmadzadeh, S. Rohani, Cellulose acetate/Plerixafor wound dressings for transplantation of menstrual blood stem cells: potential treatment modality for diabetic wounds, Journal of Drug Delivery Science and Technology 71 (2022), 103319.